Deep Resources Engineering 2 (2025) 100172

Contents lists available at ScienceDirect

Deep Resources Engineering

journal homepage: www.keaipublishing.com/en/journals/deepre/

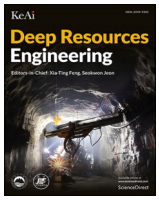

Full Length Article

Mechanics and nonlinear crack evolution of fractured sandstone under triaxial stress

Huarui Hu [a,b], Xiang Zhang [e], Jun Lu [a,b,*], Chun Zhu [d], Shiwei Liu [c]

[a] State Key Laboratory of Intelligent Construction and Healthy Operation and Maintenance of Deep Underground Engineering, Shenzhen University, Shenzhen 518060, China
[b] Guangdong Provincial Key Laboratory of Deep Earth Sciences and Geothermal Energy Exploitation and Utilization, Institute of Deep Earth Sciences and Green Energy, College of Civil and Transportation Engineering, Shenzhen University, Shenzhen 518060, China
[c] State Key Laboratory of Coal Mine Disaster Dynamics and Control, School of Resources and Safety Engineering, Chongqing University, Chongqing 400044, China
[d] School of Earth Sciences and Engineering, Hohai University, Nanjing 210098, China
[e] Department of Energy and Power Engineering, Tsinghua University, Peking 100084, China

ARTICLE INFO

Keywords : :
Damage characteristics
Fractured sandstone
Triaxial test
Crack volume strain
Deep rock

ABSTRACT

The mechanical behavior of fractured rock mass is significantly different from that of intact rock mass, and it is of great significance to study the mechanical response and damage law of crack rock to clarify the occurrence mechanism of deep geological disasters. Based on this, this paper prepared samples with cracks of different angles, simulated deep stress environment, and conducted triaxial compression test on the samples. Combined with crack strain theory and energy dissipation theory, the mechanical failure characteristics of the sample were analyzed. The results indicate that fractures significantly weaken the mechanical properties of the samples, with the strength of fractured rock decreasing by 53.85–64.67 % compared to intact rock, and the strength of fractured sandstone samples slightly increases as the crack angle increases. The evolution of crack volume strain reflects the damage and failure processes of the rock, while the slope of the crack volume strain curve indicates the rate of crack growth. The crack initiation stress and damage stress divide the crack volume strain process into the crack closing compaction stage, linear elastic deformation stage and stable expansion stage. With the crack angle increases, both crack initiation stress and damage stress initially decrease and then increase. The sample with an angle of 45° is the smallest, and the sample with an angle of 90° is the largest, indicating that the sample with a prefabricated angle of 45° is the most prone to failure. A mechanical crack propagation model was established to analyze the propagation behavior of the cracks, and the deflection propagation characteristics of the fractured sandstone are explained. Using damage mechanics and statistical theory, a multi-parameter damage evolution expression is developed. It is found that the slow damage growth stage of the sample with the crack angle of 45° lasted the longest and exhibited the fastest damage growth rate, explaining why it is most prone to failure. The evolution trends of total absorbed energy, elastic strain energy, and dissipated strain energy closely align with the stages of microcrack evolution in the sandstone samples. The evolution of energy dissipation reflects the overall damage and failure trends of the sample, and the theoretical model developed can characterize the damage and failure characteristics at a certain stage. Finally, based on the law of crack volume strain, a constitutive model for specimen damage and failure is developed, which is consistent with the test results, thereby verifying its accuracy.

1. Introduction

With the depletion of shallow resources, deep mining will become the norm of energy development in the future [1,2]. Sandstone, as a sedimentary rock widely distributed in depth, contains a lot of mineral resources and is very common in the process of resource exploitation. Under the influence of deep stress environment, the failure characteristics of sandstone are significantly different from those of shallow sandstone, it is easy to induce disasters such as rock burst, strong ore pressure and floor heave, which seriously affect the stability of

* Corresponding author at: State Key Laboratory of Intelligent Construction and Healthy Operation and Maintenance of Deep Underground Engineering, Shenzhen University, Shenzhen 518060, China
E-mail address: junlu@szu.edu.cn (J. Lu).

https://doi.org/10.1016/j.deepre.2025.100172
Received 9 December 2024; Received in revised form 12 February 2025; Accepted 11 March 2025
Available online 16 March 2025

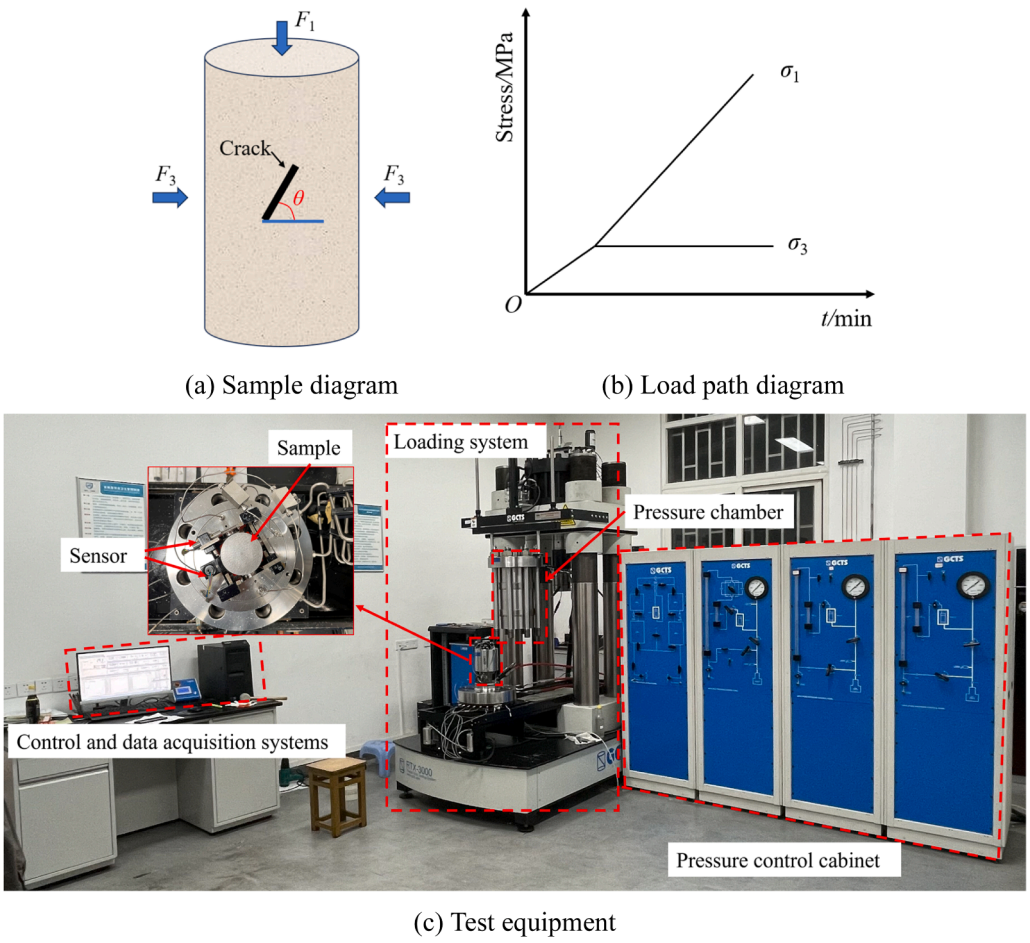

Fig. 1. Schematic diagram of Sample, test scheme and equipment.

underground engineering [3–5]. Sandstone is a naturally fissured material, and its strength characteristics, mechanical properties, and failure modes under deep stress environments exhibit distinct differences compared to shallow sandstone [6–8]. Therefore, it is of great significance for deep engineering to study the mechanical behavior and damage mechanism of fractured rock in deep environment.

Currently, both domestic and international experts and scholars have conducted extensive research on the mechanical behavior of deeply fractured rock, yielding a series of results. Existing research is primarily focused on experimental and theoretical approaches. Gong et al. [9] analyzed the damage and failure characteristics of samples during uniaxial compression testing based on energy dissipation theory, developed a constitutive model to characterize rock damage and failure, and verified its accuracy. Chen et al. [10] conducted uniaxial compression tests on rock samples of varying sizes, studied the relationship between sample size and elastic modulus, and explored the influence of sample shape and size on rock bursts. Chen et al. [11] captured the fracture signals of rock samples during the uniaxial compression failure process using acoustic emission, and examined the influence of surface cracks on the mechanical properties of the samples. As the test system continues to develop, it has become apparent that the influence of lateral stress on the mechanical properties of rock cannot be overlooked, prompting further in-depth research. Luo et al. [12], based on energy dissipation theory, investigated the conversion relationship between the energy absorbed before the peak strength of samples under varying confining pressures, dissipated energy, and properties, and explored the evolution of rock damage characteristics under different confining pressures. Li et al. [13] used 3D printing technology and triaxial compression test to study the influence of crack geometry parameters and confining pressure on the failure morphology of the sample. Janeček et al. [14] experimentally studied the failure law of samples under different triaxial stress paths, and found that the deformation response characteristics of sandstone samples under different stress paths were significantly different. Zhang et al. [15] designed a true triaxial mechanics test to study the effect of the second principal stress on rock expansion and deformation, and proposed a rock dilatancy Angle model to reveal the dilatancy characteristics of rock triaxial stress. Wang et al. [16] studied the influence of rock cementation and intermediate principal stress on the failure mechanism of the sample through true triaxial mechanics tests, and divided the sample into three modes of structure-induced failure, structure-stress-induced failure, and stress-induced failure according to the failure characteristics of the sample. Abdellah et al. [17] analyzed the variation law of rock ultimate compressive strength under different incremental displacements and confining compressive stresses under uniaxial and triaxial compression conditions through numerical simulation. Liu et al. [18] simulated and analyzed the influence of excavation on the stability of surrounding rock by using dynamic and finite element methods. Feng et al. [19] constructed a numerical model based on rock CT scan data, simulated, and analyzed rock mechanical response and fracture characteristics under uniaxial compression. Deng et al. [20] simulated and analyzed the influence of sample materials on the fracture behavior during uniaxial and triaxial compression using finite-discrete element method, and compared and verified the results of laboratory tests. The above analysis demonstrates that both physical testing and numerical simulation methods are widely used in the study of rock damage and failure mechanisms. However, the conclusions typically drawn are often specific to particular cases. To make the research results more universal, constitutive models that integrate rock damage and

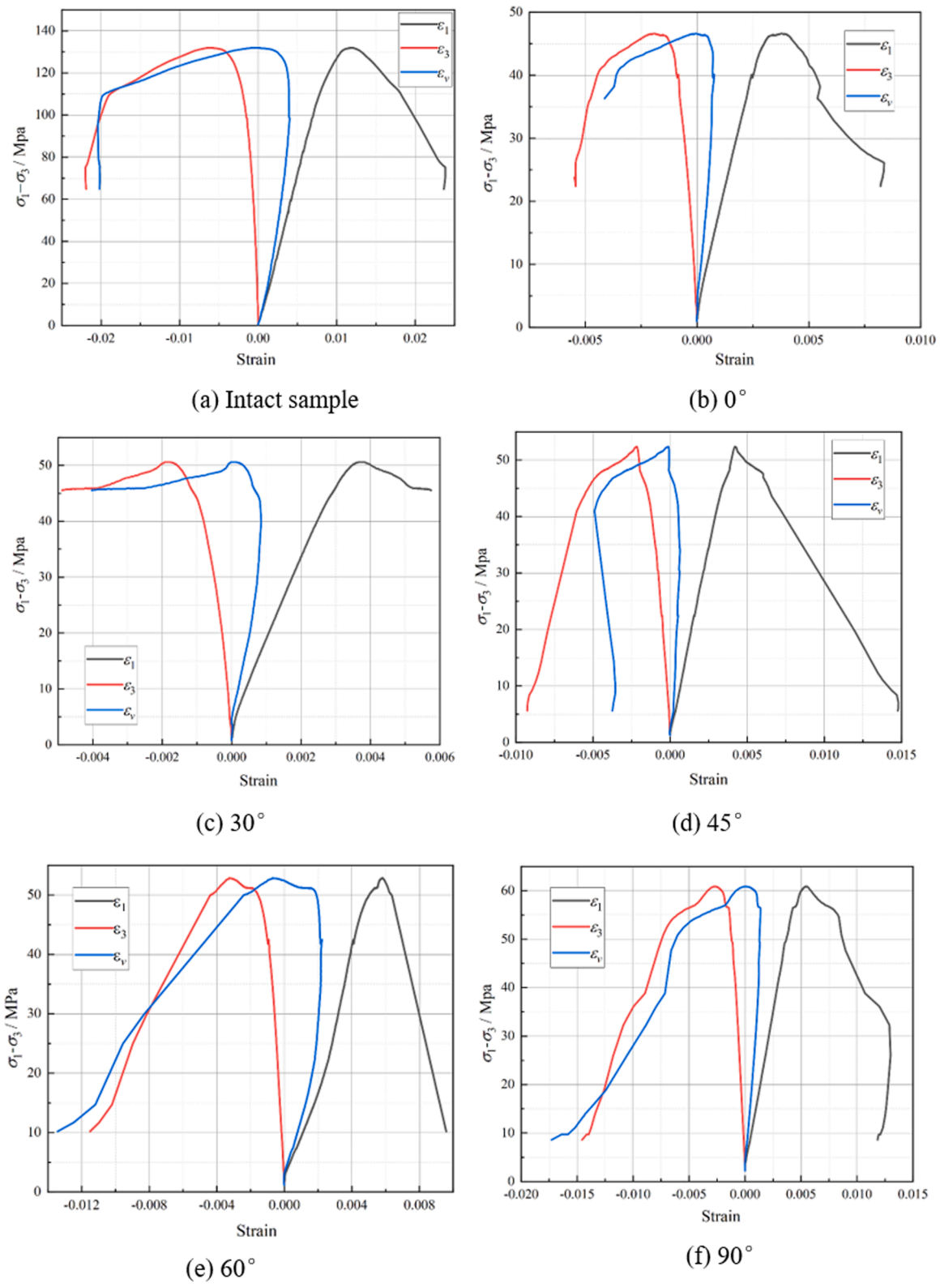

Fig. 2. Stress-strain curves of the samples.

failure with experimental results have become an important tool for revealing the internal mechanisms of rock failure [21–25]. This brief literature review demonstrates that studying rock mechanical characteristics through physical testing and theoretical analysis is an effective approach. Experimental studies can directly observe the rock failure process and further investigate its evolution using acoustic emission and high-speed cameras. However, most existing studies primarily describe or explain experimental phenomena [26–29]. Rock damage and failure result from the initiation, expansion, and convergence of cracks. By analyzing the evolution of crack strain, the corresponding thresholds of crack progression at each stage of rock stress and strain can be defined, which helps to better reveal the internal mechanical behavior of crack

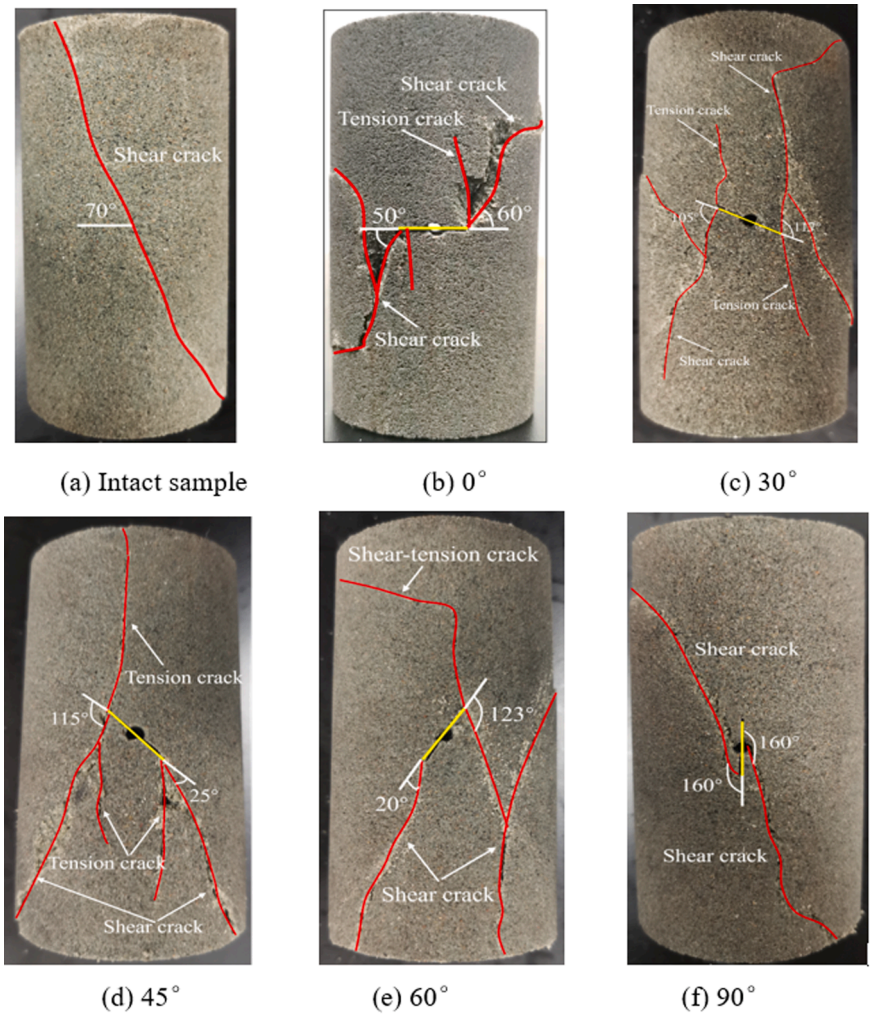

Fig. 3. Failure mode of fractured sandstone samples.

growth and the mechanism of rock damage and failure during progressive failure [30–33].

Building on this, the influence of crack angle on the variations in rock damage and failure characteristics under deep stress conditions is analyzed. First, the test samples and the testing procedure are briefly introduced. Second, using fracture mechanics theory and the principle of energy dissipation, the mechanical behavior characteristics of rock failure are analyzed, and the evolution of crack propagation during the test is discussed. Finally, a constitutive model for damage and failure of fractured rock under conventional triaxial compression is developed, and the model's accuracy is verified. This study provides theoretical guidance for the implementation of deep underground engineering.

2. Triaxial compression experiment tests

To avoid the influence of primary cracks within the rock on the test results, the samples were obtained from a single sandstone block with uniform texture. The rock blocks were processed into standard cylinders with dimensions Φ50 mm × 100 mm after cutting and polishing. The parallelism, surface error, and perpendicularity of the specimen faces are controlled within ± 0.02 mm to comply with international standards for rock mechanics specimens. After cutting and grinding, the sample is slit with prefabricated crack angles of 0°, 30°, 45°, 60°, and 90°, respectively. The crack length was 15 mm, and the crack width is 0.5 mm. The specimen and its loading configuration are shown in Fig. 1 (a).

Based on relevant studies, the axial and confining pressures are set to 15 MPa to simulate deep stress conditions. The tests were carried out on High Temperature and High-Pressure Rock Test System (GCTS RTX-3000) (Fig. 1 (c)). The loading procedure is as follows: First, the axial and confining pressures are simultaneously applied to 15 MPa by means of stress control, with a loading rate of 1 MPa/min. Then, with the confining pressure held constant, the extensometer reading is reset to zero; the displacement control method is used to increase the axial stress until failure of the sandstone samples, with a loading rate of 0.1 mm/min. The stress loading path is illustrated in Fig. 1 (b).

3. Experimental results

3.1. Characteristics of the stress-strain curves for fractured sandstone samples

The stress-strain curves of intact sandstone samples and fractured sandstone samples are shown in Fig. 2. As shown in the figure, the strength of the intact sandstone sample is significantly higher than that of the fractured sandstone samples. The strength of the intact sandstone sample is approximately 130 MPa, while the strength of the fractured sandstone samples ranges between 45 and 60 MPa. However, the strength of the fractured samples increases gradually with the increase in crack angle. The axial strain, lateral strain, and volumetric strain of the sample during loading follow a similar trend to the stress variation. During the hydrostatic pressure stage, the internal cracks of the sample

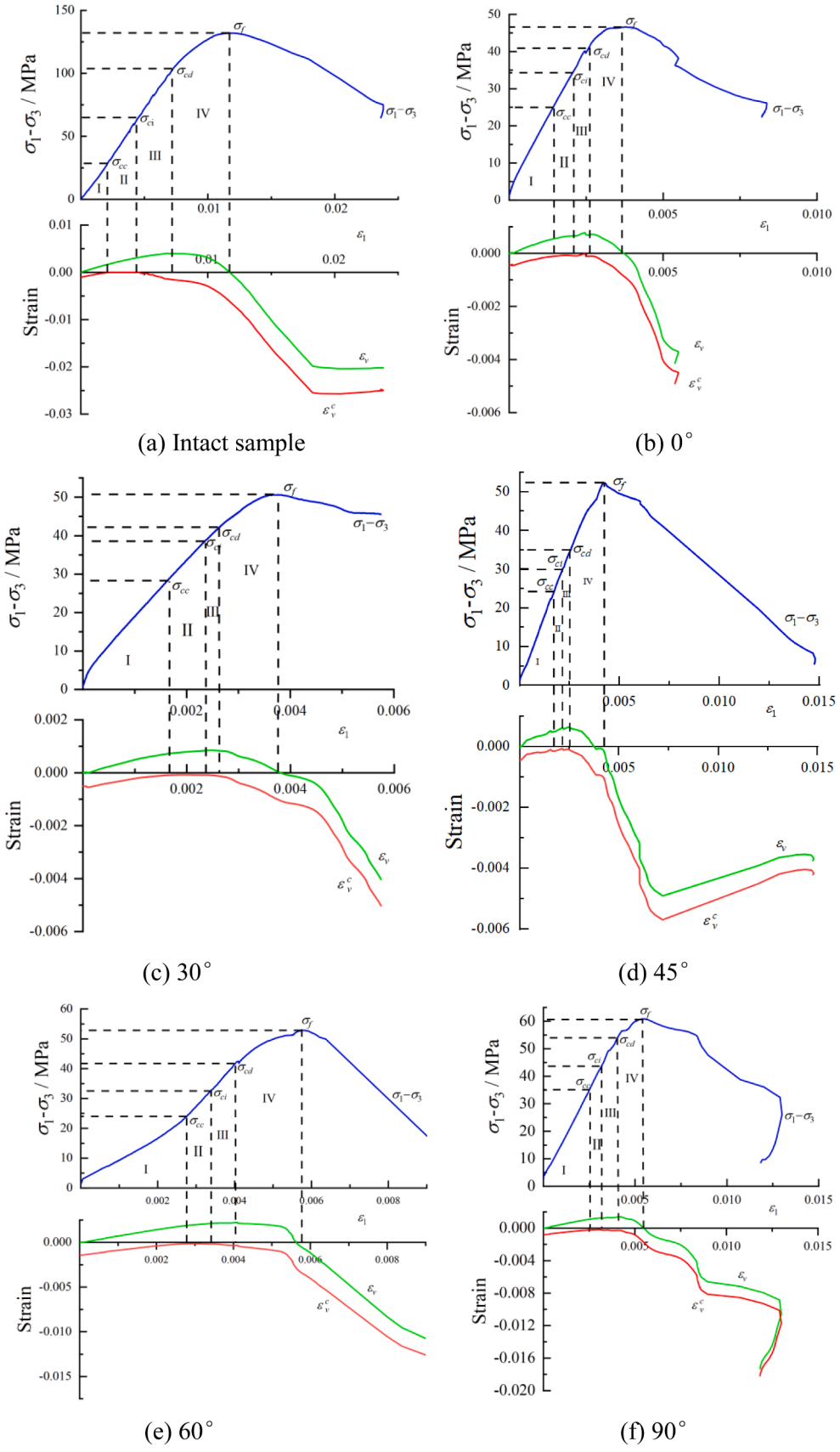

Fig. 4. Variation of crack volume strain.

are compacted, which makes the crack compaction stage less apparent in the stress-strain curve. The stress-strain curve follows a regular pattern of up-concave, approximately linear, down-concave, and drop, resembling an inverted "V" shape. The curves for lateral strain and volumetric strain with respect to stress exhibit similar shapes. However, lateral deformation is negative throughout the entire test, indicating dilatation in the sample, with increasing dilatational deformation as loading progresses. Volumetric strain is influenced by both axial and lateral strains. Since the axial strain is larger than the lateral strain, the volumetric strain is positive in the early stage. In the later stages, lateral deformation exceeds axial deformation, resulting in negative volumetric strain until specimen failure.

It can be seen from Fig. 2 that the stress-strain curve of the fractured sandstone sample initially drops and then rises, forming a zigzag pattern (Fig. 2(b)(d)), or an inflection point appears in the stress-strain curve (Fig. 2(c)(e)(f)). This behavior occurs because the cracks inside the sample are rapidly compacted under high stress, causing a sudden compression of the sample, after which the stress gradually increases.

3.2. Characteristics of the failure patterns for fractured sandstone samples

The failure mode diagram of the sample is shown in Fig. 3. Shear failure is observed in intact samples, whereas tensile-shear composite failure predominantly occurs in fractured sandstone. The crack morphology of fractured sandstone samples differs significantly from that of intact sandstone, exhibiting more complex crack forms, which result in the formation of both tension and shear cracks.

The intact sandstone is pure shear failure, and the angle between the fracture plane and the horizontal direction is 70°. The crack at the crack tip of sandstone samples with an angle of 0° is complicated, and there are fragments spalling at the tip, and two shear cracks are mainly formed, with initiation angles of 55° and 60° respectively. As the crack angle increases, the angle between the fracture plane and the prefabricated crack plane becomes progressively larger, ranging from 50° to 160°. When the prefabricated crack angle exceeds 30°, shear crack deflection occurs. The maximum deflection angles for samples with crack angles of 30°, 45°, and 60° are 117°, 115°, and 123°, respectively. In contrast, the deflection angle of samples with a 90° crack angle is 160°, with no apparent tension cracks on the specimen surface. Based on the deformation and failure characteristics, an increase in the prefabricated crack angle results in a shift from brittle to plastic failure. However, the tension cracks at both ends of the prefabricated cracks did not propagate through the sample to form a penetrating fracture plane.

3.3. Crack propagation behavior

The damage and deformation of rock during loading result from the initiation and development of microcracks [34–36]. Microcracks continuously form during the loading process, and their propagation and penetration ultimately lead to the macroscopic failure of the rock. Therefore, from a microscopic perspective, the axial and circumferential deformation of sandstone samples result from the initiation and development of microcracks, and crack strain can describe the evolution process of microcracks in rocks.

The strain in the test process can be divided into elastic strain caused by matrix deformation and crack strain caused by micro-cracks in the rock, which can be calculated by the following formula [34]:

$$\varepsilon_i = \varepsilon_i^e + \varepsilon_i^c \tag{1}$$

Where, ε_i, ε_i^e and ε_i^c are the total strain, elastic strain and crack strain corresponding to each principal stress direction, respectively, $i = 1,2,3$.

The formula for calculating the volume strain ε_v is:

$$\varepsilon_v = \varepsilon_1 + \varepsilon_2 + \varepsilon_3 \tag{2}$$

Where, ε_1, ε_2 and ε_3 are the strain corresponding to the direction of maximum principal stress, intermediate principal stress and minimum principal stress, respectively.

Similarly, the volume strain is composed of the crack volume strain formed by the closing of microcracks or the expansion and expansion of new cracks and the elastic volume strain formed by the matrix.

$$\varepsilon_v = \varepsilon_v^e + \varepsilon_v^c \tag{3}$$

Where, ε_v^e and ε_v^c are elastic volume strain and crack volume strain.

According to Hooke's law, the elastic strain during rock loading can be calculated as follows:

$$\begin{cases} \varepsilon_1^e = \dfrac{1}{E}[\sigma_1 - \mu(\sigma_2 + \sigma_3)] \\ \varepsilon_2^e = \dfrac{1}{E}[\sigma_2 - \mu(\sigma_1 + \sigma_3)] \\ \varepsilon_3^e = \dfrac{1}{E}[\sigma_3 - \mu(\sigma_1 + \sigma_2)] \end{cases} \tag{4}$$

Where, ε_1^e, ε_2^e and ε_3^e the corresponding elastic strain in the direction of the principal stress respectively, E and μ are the elastic modulus and Poisson's ratio in the straight-line stage of the stress-strain curve, respectively.

Under conventional triaxial loading $\sigma_2 = \sigma_3$, therefore, the elastic volume strain can be calculated as follows.

$$\varepsilon_v^e = \varepsilon_1^e + \varepsilon_2^e + \varepsilon_3^e = \frac{1-2\mu}{E}(\sigma_1 - \sigma_2) \tag{5}$$

Then the crack volume strain is,

$$\varepsilon_v^c = \varepsilon_v - \varepsilon_v^e = \frac{1-2\mu}{E}(\sigma_1 + 2\sigma_3) \tag{6}$$

The change curve of crack volume strain under conventional triaxial loading is shown in Fig. 4. The figure clearly reflects the evolution process of micro-cracks. According to the volume strain and crack volume strain of sandstone samples, there are characteristic stress thresholds in the crack evolution process in the pre-peak stage, such as crack closing stress (σ_{cc}), crack initiation stress (σ_{ci}), damage stress (σ_{cd}) and peak strength (σ_f). The threshold points divide the crack evolution process into four stages: crack compaction, elastic compression, steady crack growth, and crack acceleration growth. It was observed that the initial crack closing stage lasts longer in fractured sandstone samples than in intact samples, with the shortest duration occurring at a crack angle of 45° and the longest at 90°. As stress continues to increase, it does not reach the threshold required for microcrack initiation, causing the crack volume strain curve to remain approximately horizontal. At this stage, few or no microcracks are present, and the volume strain of sandstone samples results from the elastic volume strain caused by matrix deformation. During this stage, intact sandstone samples exhibit a longer duration than fractured sandstone samples. When the prefabricated crack angle is 45°, the elastic stage duration is the shortest, while at a 0° crack angle, the duration is the longest.

When the applied stress exceeds the threshold required for microcrack initiation, microcrack initiation and propagation commence, as evidenced by the increase in crack volume strain. Because crack initiation and propagation are an expansion process, the crack volume strain is negative. The elastic volume strain caused by the matrix increases linearly, causing the growth rate of volume strain to decelerate. At this stage, intact sandstone samples exhibit a longer duration than prefabricated fractured sandstone samples. When the prefabricated crack angle is 30°, the duration of the stable crack growth stage is the shortest, while at crack angles of 60° and 90°, the duration is the longest. When the applied stress surpasses the elastic volume strain caused by matrix compression, the sandstone sample transitions from volume compression to volume expansion at the macroscopic level. The rock begins to expand, the volume strain decreases, and the stress-strain curve becomes nonlinear. Ultimately, the cumulative cracks within the specimen

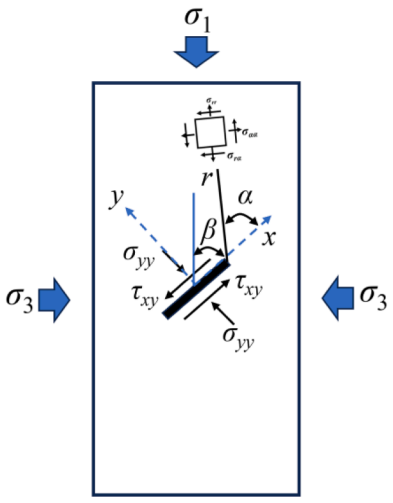

Fig. 5. Mechanical model of crack growth under pressure.

coalesce to form penetrating cracks, leading to sample failure. It is important to note that, because the sample underwent loading during the hydrostatic pressure stage, the internal cracks were compacted. However, the stress-strain behavior during the loading stage is primarily analyzed in the figure, which is why the crack compaction stage is not clearly observed in Fig. 4.

4. Discussion

4.1. Analysis of failure characteristics

Fig. 5 shows the mechanical model of crack propagation in sandstone samples under pressure. A prefabricated inclined crack with length L is introduced at the center of the sandstone sample, with an angle β between the crack and the axial direction. A planar rectangular coordinate system xOy is defined with the crack center as the origin. The X-axis is parallel to the direction of the prefabricated crack, while the Y-axis is perpendicular to it.

The relationship between the stress on the prefabricated crack surface and the axial stress and the circumferential stress is,

$$\begin{cases} \sigma_{yy} = \sigma_1 \sin^2\beta + \sigma_3 \cos^2\beta \\ \tau_{xy} = (\sigma_1 - \sigma_3)\sin\beta\cos\beta \end{cases} \tag{7}$$

Where, $\sigma_{yy}$is the normal stress on the crack surface, MPa; $\tau_{xy}$is the shear stress on the crack surface, MPa.

Due to the friction effect, the normal stress on the prefabricated crack surface will form friction τ_f and reduce the shear stress on the crack surface, so the effective shear stress on the crack surface is:

$$\begin{aligned} \tau_{eff} &= \tau_{xy} - \tau_f = \tau_{xy} - f\sigma_{yy} \\ &= (\sigma_1 - \sigma_3)\sin\beta\cos\beta - f\left(\sigma_1 \sin^2\beta + \sigma_3 \cos^2\beta\right) \end{aligned} \tag{8}$$

Where, f is the friction coefficient.

When a non-closed crack is pressurized, the crack tip is subjected to the joint action of tensile stress and shearing stress, so the crack tip stress field can be calculated according to the following formula:

$$\begin{cases} \sigma_{rr} = \dfrac{1}{2\sqrt{2\pi r}} \cos\left[K_{\mathrm{I}} \cos\dfrac{\alpha}{2}(3 - \cos\alpha) + K_{\mathrm{II}} \sin\dfrac{\alpha}{2}(3\cos\alpha - 1)\right] \\ \sigma_{\alpha\alpha} = \dfrac{1}{2\sqrt{2\pi r}} \cos\dfrac{\alpha}{2}\left[K_{\mathrm{I}}(\cos\alpha + 1) - 3K_{\mathrm{II}} \sin\alpha\right] \\ \sigma_{r\alpha} = \dfrac{1}{2\sqrt{2\pi r}} \cos\dfrac{\alpha}{2}\left[K_{\mathrm{I}} \sin\alpha + K_{\mathrm{II}}(3\cos\alpha - 1)\right] \end{cases} \tag{9}$$

Where, α is the polar angle and r is the distance between the microelement and the tip of a single crack. K_{I} and K_{II} are the stress intensity factors of tensile crack and shear crack, respectively.

According to the theory of fracture mechanics, the stress intensity factor at the tip of the central inclined crack is [37],

$$\begin{cases} K_{\mathrm{I}} = \sigma_{yy}\sqrt{\pi a} = \left(\sigma_1 \sin^2\beta + \sigma_3 \cos^2\beta\right)\sqrt{\pi a} \\ K_{\mathrm{II}} = \tau_{eff}\sqrt{\pi a} = \left[(\sigma_1 - \sigma_3)\sin\beta\cos\beta - f\left(\sigma_1 \sin^2\beta + \sigma_3 \cos^2\beta\right)\right]\sqrt{\pi a} \end{cases} \tag{10}$$

According to the maximum circumferential tensile stress criterion, if the crack spreads in the direction of α, the following conditions need to be met.

$$\begin{cases} \dfrac{\partial \sigma_{\alpha\alpha}}{\partial \alpha}\Big|_{\alpha=\alpha_0} = 0 \\ \dfrac{\partial^2 \sigma_{\alpha\alpha}}{\partial \alpha^2}\Big|_{\alpha=\alpha_0} < 0 \end{cases} \tag{11}$$

That is, the expression in formula (9) is 0 after partial derivative of $\sigma_{\alpha\alpha}$,

$$\cos\frac{\alpha}{2}\left[K_{\mathrm{I}} \sin\alpha + K_{\mathrm{II}}(3\cos\alpha - 1)\right] = 0 \tag{12}$$

When $\cos(\alpha/2) = 0$, the second order partial differential is greater than 0, which does not meet the conditions of formula (11), so the crack initiation Angle should meet:

$$\left[K_{\mathrm{I}} \sin\alpha + K_{\mathrm{II}}(3\cos\alpha - 1)\right] = 0 \tag{13}$$

According to formula (13), the value of crack initiation Angle α depends on K_{I} and K_{II}.

When $K_{\mathrm{II}} = 0$, the crack belongs to tension crack, and $\alpha = 0^\circ$, the crack extends along the prefabricated crack extension direction.

When $K_{\mathrm{I}} = 0$, the crack belongs to pure shear crack, and the crack initiation angle $|\alpha| = 70.5^\circ$.

When $K_{\mathrm{I}} \neq 0$, $K_{\mathrm{II}} \neq 0$, it can be obtained by formula (13):

$$\alpha = 2\arctan\frac{K_{\mathrm{I}} \Big/ K_{\mathrm{II}} \pm \sqrt{(K_{\mathrm{I}}/K_{\mathrm{II}})^2 + 8}}{4} \tag{14}$$

According to the maximum circumferential tensile stress criterion, the cause of tensile crack can be explained, but there is no way to explain the cause of deflection shear crack.

For the deflection shear crack, the maximum radial shear stress criterion can be used. According to formula (9), the first and second partial derivatives of α should meet the following conditions:

$$\begin{cases} \dfrac{\partial \sigma_{\alpha\alpha}}{\partial \alpha}\Big|_{\alpha=\alpha_{\mathrm{II}}} = 0 \\ \dfrac{\partial^2 \sigma_{r\alpha}}{\partial \alpha^2}\Big|_{\alpha=\alpha_{\mathrm{II}}} < 0 \end{cases} \tag{15}$$

The calculation result is $a_{\mathrm{II}} = 0^\circ$or $|\ a_{\mathrm{II}}| = 123.8^\circ$。

4.2. Characteristics of the energy evolution for samples

During the testing process, the energy exchange between the sandstone sample and its external environment can be considered dynamically conserved, with energy continually redistributed within the sample. The testing environment is maintained at room temperature, and heat radiation and conduction are negligible. As a result, the mechanical energy input is primarily converted into elastic strain energy and plastic strain energy. Consequently, the following formula can be derived.

$$U = U^d + U^e \tag{16}$$

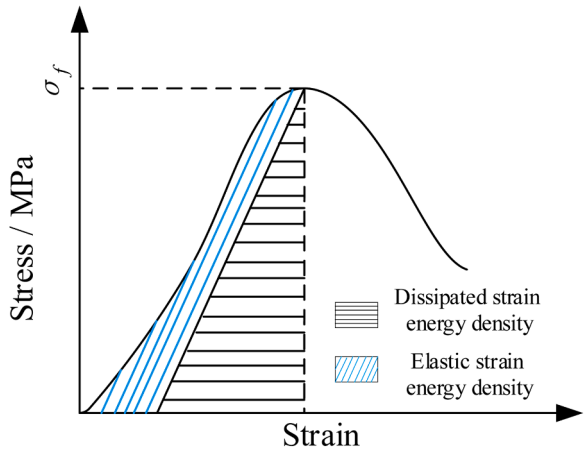

Fig. 6. Calculation diagram of elastic strain energy and dissipative strain energy based on stress-strain curve.

Where, U, U_d and U_e is the total energy input per unit volume of rock, dissipated energy, and stored energy when elastic deformation occurs, MJ/m^3. Based on the stress-strain relationship and the corresponding strain energy calculation method, the calculation methods of U_d and U_e are shown in Fig. 6.

It is assumed that the interior of the rock is homogeneous and isotropic during loading. According to the elastic theory, the expression of elastic strain energy density during loading is as follows:

$$U^e = \frac{1}{2}(\sigma_1\varepsilon_1 + \sigma_2\varepsilon_2 + \sigma_3\varepsilon_3) \tag{17}$$

The following formula is obtained from generalized Hooke's law.

$$\begin{cases} \varepsilon_1 = \frac{1}{E}[\sigma_1 - \mu(\sigma_2 + \sigma_3)] \\ \varepsilon_2 = \frac{1}{E}[\sigma_2 - \mu(\sigma_1 + \sigma_3)] \\ \varepsilon_3 = \frac{1}{E}[\sigma_3 - \mu(\sigma_1 + \sigma_2)] \end{cases} \tag{18}$$

Substitute the formula (18) into the formula (17):

$$U^e = \frac{1}{2E}\left[\sigma_1^2 + \sigma_2^2 + \sigma_3^2 - 2\mu(\sigma_1\sigma_3 + \sigma_2\sigma_3 + \sigma_1\sigma_3)\right] \tag{19}$$

For conventional triaxial loading, formula (19) can be written as follows:

$$U^e = \frac{1}{2E}\left[\sigma_1^2 + 2\sigma_3^2 - 2\mu\left(2\sigma_1\sigma_3 + \sigma_3^2\right)\right] \tag{20}$$

In a conventional triaxial loading test, hydrostatic pressure induces compressive deformation in sandstone samples, thereby performing positive work on the samples. When the axial stress exceeds the confining stress, axial deformation in the sandstone samples exhibits compressive characteristics, while the circumferential deformation shows expansive characteristics. The circumferential stress resists the expansion of the sandstone samples, leading to positive work performed by the axial stress and negative work performed by the circumferential stress. The total energy density of the sandstone samples during loading can be calculated using the following formula.

$$U = U_1 + 2U_3 + U_0 \tag{21}$$

Where U_1, U_3 and U_0 are respectively the strain energy density of axial stress, circumferential stress, and hydrostatic pressure work, MJ/m^3.

$$U_0 = \frac{3(1-2\mu)}{2E}\sigma_3^2 \tag{22}$$

During the test, the work done by the external force is transformed into the axial strain energy density U_1 and the circumferential strain energy density U_3, which are obtained according to the integral of the stress-strain curve.

$$\begin{cases} U_1 = \int_0^{\varepsilon_1^t} \sigma_1 d\varepsilon_1 \\ U_2 = \int_0^{\varepsilon_3^t} \sigma_3 d\varepsilon_3 \end{cases} \tag{23}$$

Where, ε_1^t is the axial strain at time t; $\varepsilon_3^t$is the toroidal strain at time t.

$$U^d = U_1 + 2U_3 + U_0 - U^e \tag{24}$$

Based on the above formulas and combined with conventional triaxial test data, the strain energy density of sandstone samples under conventional triaxial loading was calculated, as shown in Fig. 7.

As shown in Fig. 7, the variation trend of strain energy density in sandstone samples is consistent. With the continuous application of axial stress, the input strain energy density increases progressively, with elastic strain energy density initially dominating, while dissipative strain energy density remains relatively small under low stress conditions. Once the stress exceeds the yield stress, the dissipative strain energy density increases rapidly, while the growth rate of elastic strain energy density begins to decline. This evolution of energy density aligns with the stages of microcrack development.

The energy evolution behavior of fractured sandstone samples generally mirrors that of intact sandstone samples. However, during the initial loading stage, the input energy is predominantly converted into dissipative strain energy, with the density of dissipative strain energy being higher than that of elastic strain energy. This suggests that the energy dissipated due to crack closure in fractured sandstone during the initial crack compaction stage is greater than in intact sandstone samples. Nevertheless, the stress after micro-crack closure does not reach the threshold required for micro-crack propagation, and as a result, the energy dissipation stabilizes at a fixed value. At this stage, energy dissipation primarily occurs through the friction of microcracks. When the stress exceeds the stress condition required for microcrack initiation, the evolution law of strain energy density in subsequent stages is basically consistent with the change trend of intact sandstone samples. However, due to the existence of prefabricated cracks, the strain energy density of fractured sandstone samples is much smaller than that of intact sandstone samples. Taking the peak stress as an example, the strain energy density of intact sandstone samples is 4–7 times that of fractured sandstone samples, which essentially explains the weakening effect of prefabricated cracks on sandstone samples.

Especially after the peak stress, the rapid expansion of macroscopic cracks lead to specimen failure, causing a sharp decrease in the bearing capacity of the sandstone specimen. The axial strain of the sandstone specimen continues to increase under compressive stress, resulting in a continuous rise in total strain energy density. The dissipative strain energy density increases rapidly, while the elastic strain energy density begins to decrease. However, the sample with a crack angle of 30° still maintains a high residual strength after the peak value and does not break rapidly, so the dissipative energy does not increase rapidly (Fig. 7 (c)). This suggests that when rocks lose their load-bearing capacity, previously stored elastic strain energy is released and converted into other forms of energy. In cases where the rock is brittle and has a free surface, the elastic strain energy is likely converted into the kinetic energy of ejected fragments, which contributes to dynamic disasters such as rock bursts.

4.3. Analysis of specimen damage evolution

4.3.1. Damage correlation analysis

From the point of view of statistics, the damage characteristics of rock are described based on damage mechanics. If the strength law of

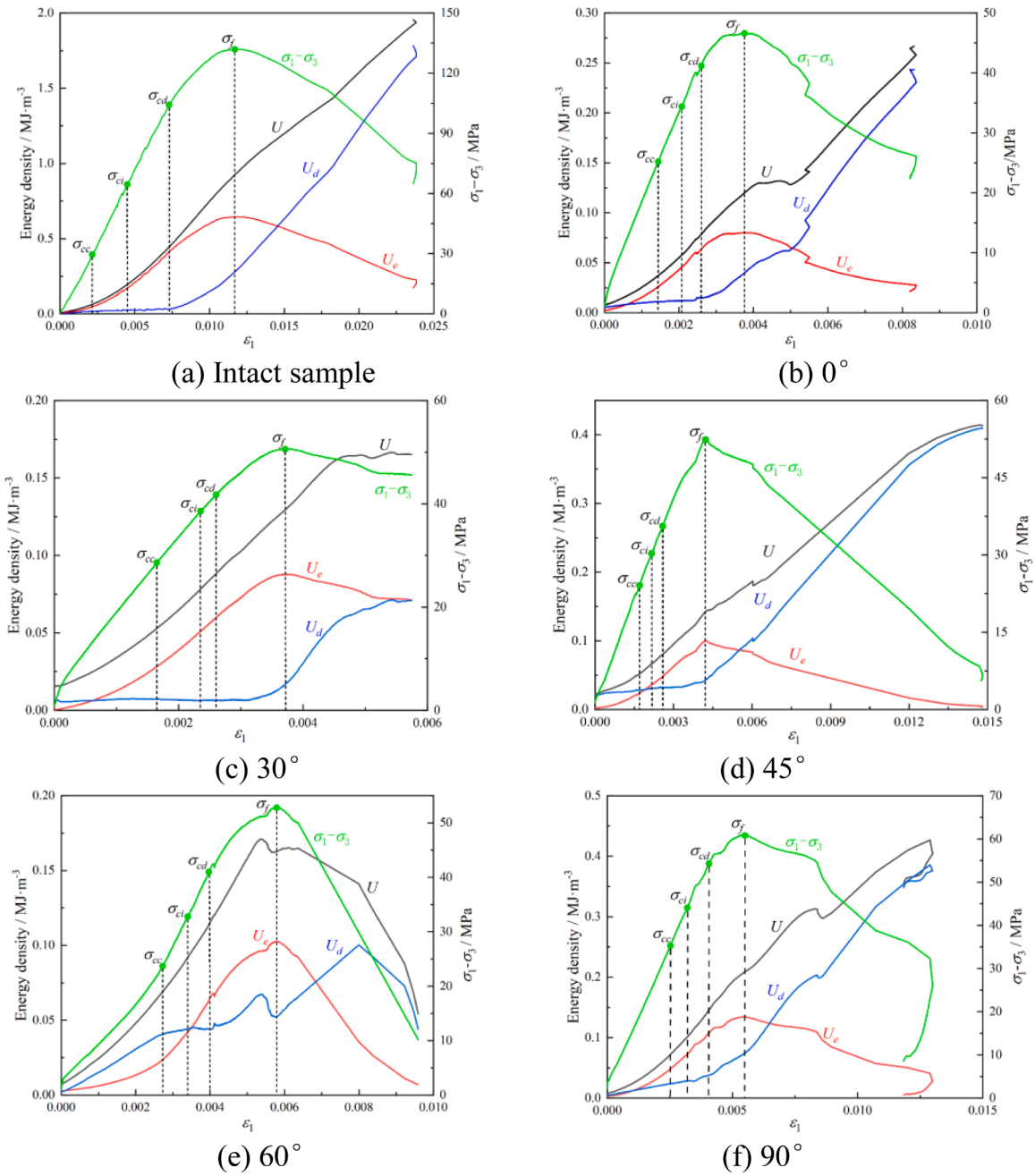

Fig. 7. Energy evolution of samples.

micro-components in rocks follows Weibull distribution, the probability density of strength distribution of rock elements can be calculated according to the following formula:

$$P(\varepsilon) = \frac{m}{\gamma}\left(\frac{\varepsilon}{\gamma}\right)^{m-1} \exp\left[-\left(\frac{\varepsilon}{\gamma}\right)^{m}\right] \tag{25}$$

Where, $P(\varepsilon)$ is the strength distribution function of the unit; ε is the strain at a certain point in the rock mass, γ and m are the damage related parameters.

The damage variable D is defined as the ratio of the number of damaged particles and the total number of particles in the rock.

$$D = \frac{h}{H} \tag{26}$$

Where, H is the total number of particles in the rock in a lossless state; h is the number of damaged particles in the rock after loading.

When the strain is ε, the number of damaged elements can be calculated by the following formula.

$$h = \int_0^{\varepsilon} HP(\varepsilon)d\varepsilon = H\left\{1 - \exp\left[-\left(\frac{\varepsilon}{\gamma}\right)^{m}\right]\right\} \tag{27}$$

Then D is,

$$D = 1 - \exp\left[-\left(\frac{\varepsilon}{\gamma}\right)^{m}\right] \tag{28}$$

When the rock is undamaged, $D = 0$; When the rock is damaged, $0 < D < 1$. In the theory of damage mechanics, the stress-strain relationship of damaged rock is defined as,

$$\sigma = E(1 - D)\varepsilon \tag{29}$$

Table 1
Damage parameters.

	Intact	0°	30°	45°	60°	90°
m	4.8668	3.9708	8.8628	20.4363	2.4135	5.3587
γ	0.0168	0.0056	0.0049	0.0048	0.0084	0.0076

Then the constitutive relation of damaged rock body under external loading is as follows.

$$\sigma = E\varepsilon \exp\left[-\left(\frac{\varepsilon}{\gamma}\right)^m\right] \tag{30}$$

Where, $\sigma$is the stress of the rock under load, which is approximately the slope of the straight section of the stress-strain curve, MPa; E is the elastic modulus of the rock in a non-destructive state, GPa; $\varepsilon$is the strain of rock under load.

$$\frac{\sigma}{E} = \varepsilon \exp\left[-\left(\frac{\varepsilon}{\gamma}\right)^m\right] \tag{31}$$

Derivation gives the following formula:

$$\frac{d\sigma}{dE}|\sigma = \sigma_f, \varepsilon = \varepsilon_f = 0 \tag{32}$$

Where, σ_f is the stress of the rock when it reaches the peak value, MPa; ε_f is the axial strain of the rock at peak stress.

Combined with the above formula, the damage related parameters m and γ are obtained :

$$m = \frac{1}{\ln\left(\frac{E\varepsilon_f}{\sigma_f}\right)} \tag{33}$$

$$\gamma = \varepsilon_f m^{\frac{1}{m}} \tag{34}$$

According to the stress, axial strain, and elastic modulus at the peak of stress-strain curve of sandstone samples under conventional triaxial loading, the damage parameters of sandstone samples with prefabricated cracks at different angles can be calculated, as shown in Table 1 below.

Assuming that one damage-related parameter is fixed, the relationship between the other damage-related parameter and sample damage is analyzed. Based on the experimental data, the damage-related parameters m and γ are calculated within the ranges of 2.4135–20.4363 and 0.0048–0.0168, respectively. For γ= 0.02 and m= 4.7, the influence of these damage-related parameters on the damage evolution curve is shown in Fig. 8.

As shown in Fig. 8 (a), the damage variable increases slowly during the initial deformation stage of the sandstone sample, and then accelerates once the deformation reaches a certain threshold. The smaller the damage-related parameter m, the shorter the flat segment, and the faster the damage variable begins to increase, although the growth rate remains slower. The parameter m represents the deformation threshold at which the rapid increase in the damage variable begins for the sandstone samples.

From Fig. 8 (b), it is evident that the damage-related parameter γ is associated with the slope of the damage variable evolution curve. The larger the value of γ, the smaller the slope of the damage variable in the pre-peak stage, indicating a slower rate of increase in the damage variable. Thus, the parameter γ can characterize the growth rate of the damage variable in sandstone samples.

4.3.2. *Damage characteristics based on energy evolution*

Rock fracture is the result of the further development of internal defects and micro-cracks under the action of stress, which is accompanied by the evolution of energy dissipation [38,39]. The dissipative strain energy of rock accumulates continuously with the increase of stress, so it can be assumed that the damage variable of sandstone is 1 when the peak stress is reached. At this time, the dissipated strain energy density is the dissipated strain energy density required for failure, and the damage variable D can be calculated by the following formula.

$$D = \frac{U_d^t}{U_d^f} \tag{35}$$

Where, U_d^tstrain energy density U is a certain dissipated strain energy density at time t, MJ/m^3; U_d^f is the dissipation at the peak stress, MJ/m^3.

The variation in damage variables of sandstone samples is shown in Fig. 9. Compared to the previous two damage analysis methods, the damage variable defined by dissipated strain energy density better accounts for the influence of prefabricated cracks on initial damage. Moreover, its variation trend is more consistent with the failure process of sandstone samples during loading. In the initial loading stage, as stress increases, cracks close, causing a slight increase in the damage variable. During the elastic compression stage, the damage variable curve remains nearly horizontal, with the damage variable either increasing slowly or remaining constant. Upon entering the rapid crack growth stage, the damage variable rises sharply, reaching its maximum value at peak strain, at which point the specimen fails.

The entire damage process of the sample can be more effectively represented through energy dissipation analysis, while the damage state

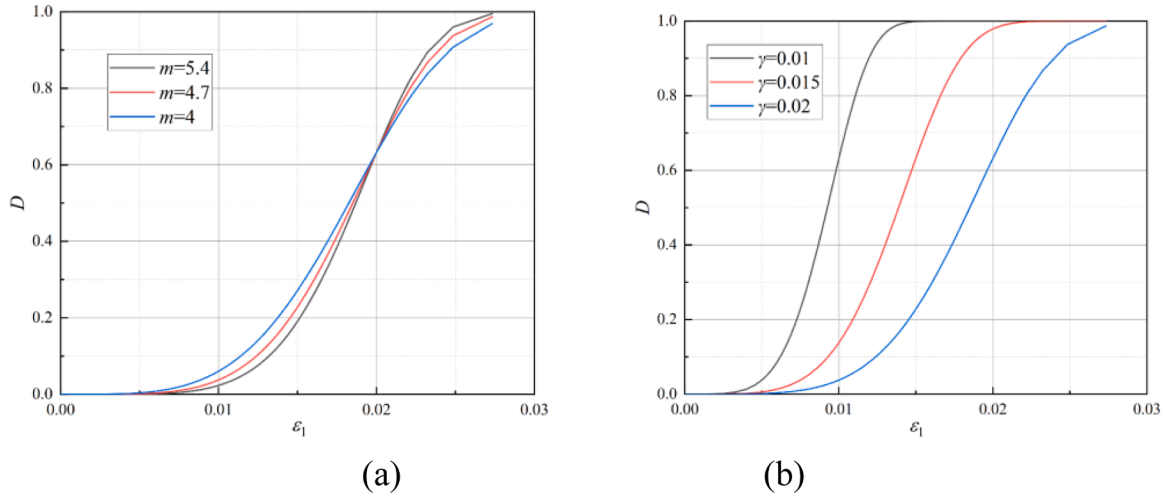

Fig. 8. Influence of damage related parameters on damage evolution curve: (a) Effect of m on damage evolution;(b) Effect of ε_0 on damage evolution.

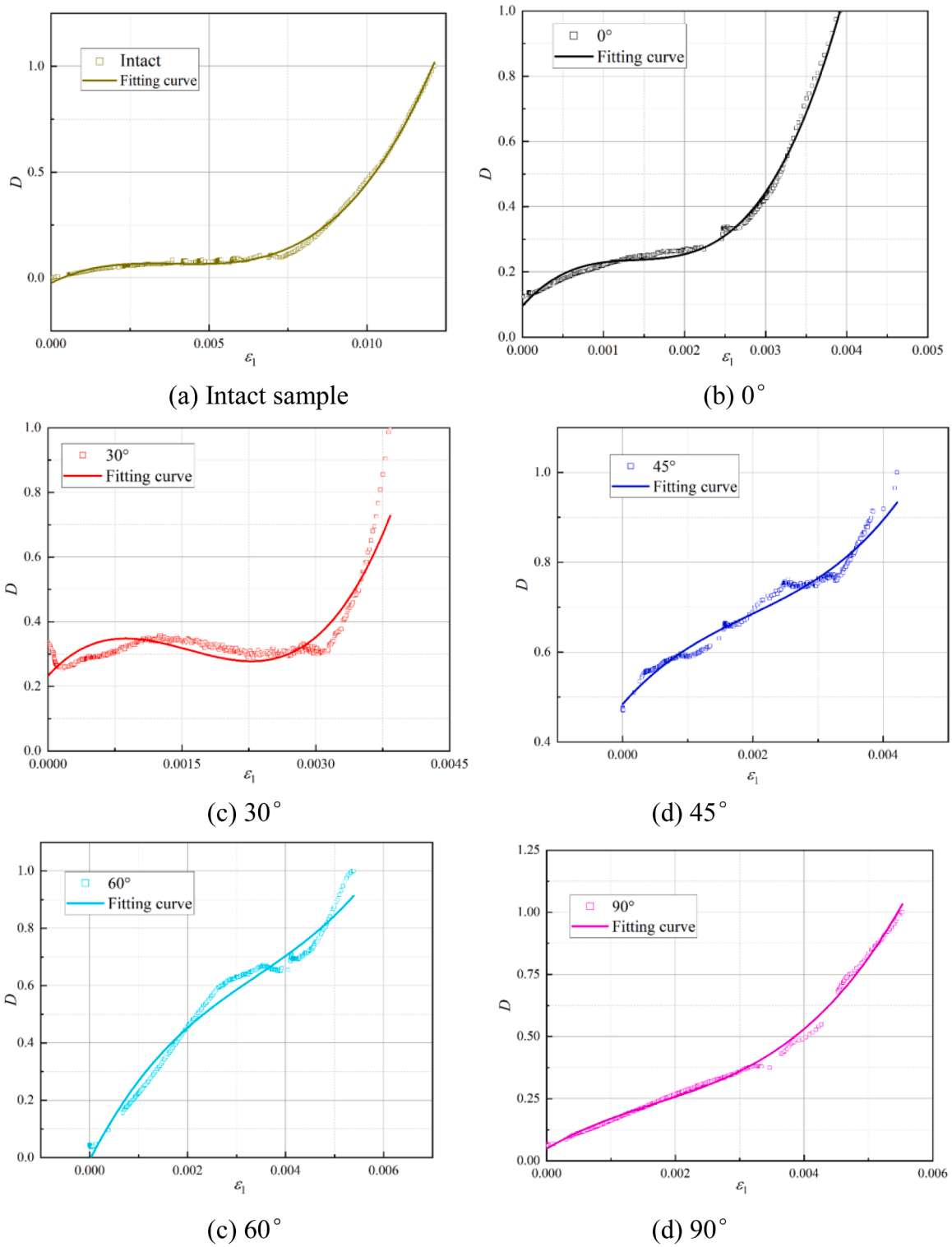

Fig. 9. Analysis of specimen damage evolution law.

of the sample under specific conditions can be more accurately analyzed using mechanical parameter analysis. These two methods can be employed to investigate the damage and failure characteristics of sandstone, with their combined strengths offering a comprehensive analysis of rock damage.

By comparing the strain energy density of the single-fracture sandstone sample at peak stress, it is observed that strain energy density increases with the prefabricated crack angle. The relationship between the prefabricated crack angle and strain energy density is shown in Fig. 10. A strong linear correlation exists between the prefabricated crack angle and strain energy density at peak stress. The goodness of fit for the total strain energy density, elastic strain energy density, and dissipative strain energy density relative to the prefabricated single crack angle are 0.92, 0.91, and 0.91, respectively. When the prefabricated single crack angle is 0°, the total strain energy density, elastic strain energy density, and dissipative strain energy density are minimal.

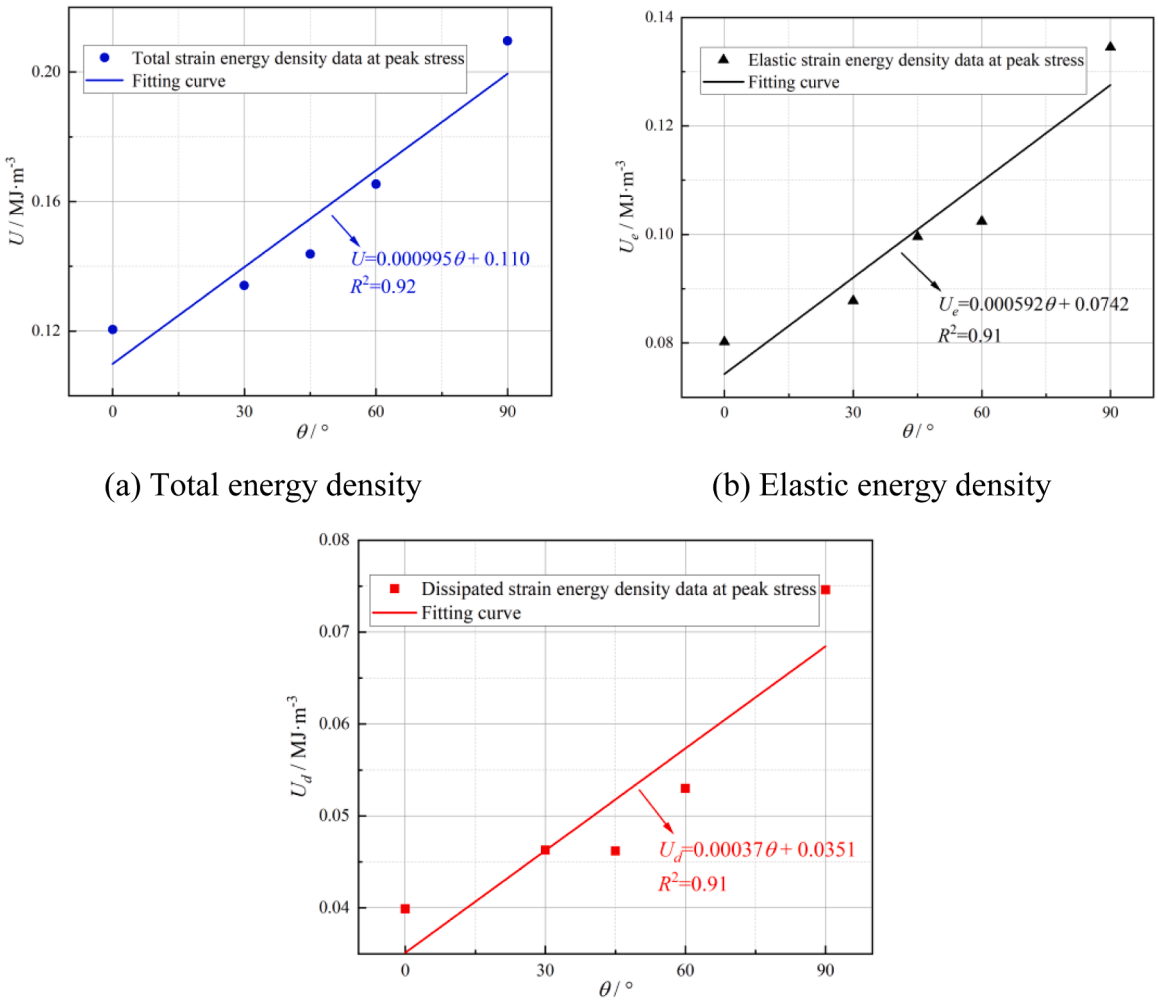

Fig. 10. Effect of crack angle on energy density of samples.

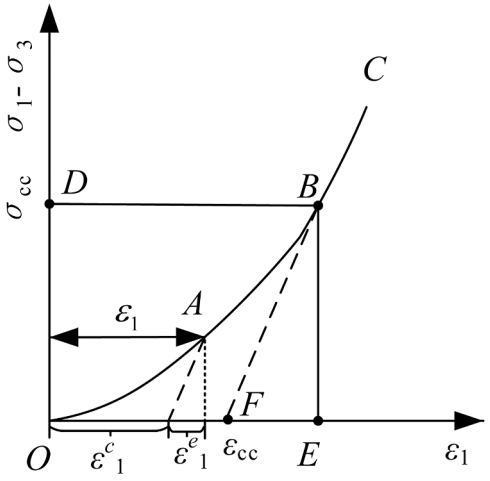

Fig. 11. Quantization diagram of axial strain at crack closing stage.

As the crack angle increases, the strain energy density increases. This also explains the phenomenon where smaller crack angles correspond to lower peak stress values.

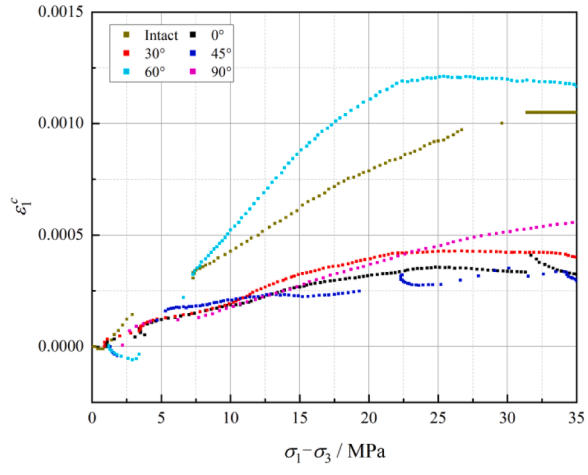

Fig. 12. Axial crack strain of fractured sandstone.

4.4. Analysis of damage constitutive model

The crack volume strain in the conventional triaxial loading process is calculated above. Similarly, the axial strain is also composed of axial

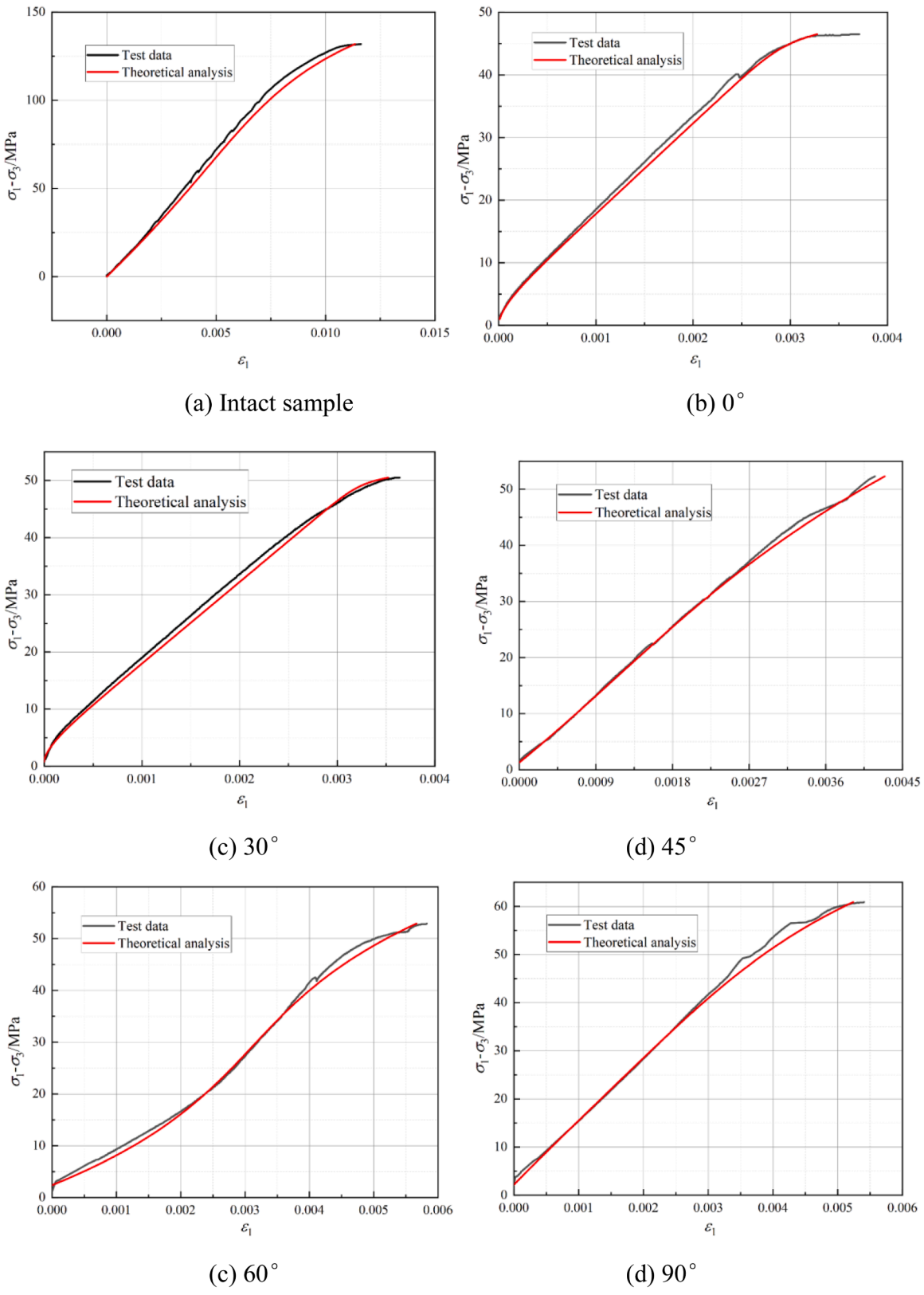

Fig. 13. Comparison between experimental data and theoretical analysis results.

elastic strain and axial crack strain, as shown in Fig. 11.

According to formula 36. It can be found that the axial crack strain increases with the stress loading process (Fig. 12), but when the stress reaches a certain value, the axial crack strain no longer increases but fluctuates up and down within a certain range, and then the axial crack is cracked. The grain strain reaches its maximum.

The axial crack strain is a function of σ_1-σ_3, and the relationship between the axial crack strain and the stress difference can be expressed by a negative exponential function.

$$\varepsilon_1^c = V_m\left[1-\exp\left(-\frac{\sigma_1-\sigma_3}{p}\right)\right] \tag{36}$$

A model can be obtained to quantitatively characterize the initial crack closure stage and elastic stage.

$$\varepsilon_1 = \frac{\sigma_1-\sigma_3}{E} + V_m\left[1-\exp\left(-\frac{\sigma_1-\sigma_3}{p}\right)\right] \tag{37}$$

Considering that the strength of sandstone samples gradually decreases due to the unsteady expansion of microcracks near the peak stress, and the elastic modulus also decreases with the expansion of microcracks. Combined with the damage variables defined above, a model that can characterize the pre-peak stage is obtained.

$$\varepsilon_1 = \frac{\sigma_1-\sigma_3}{(1-D)E} + V_m\left[1-\exp\left(-\frac{\sigma_1-\sigma_3}{p}\right)\right] \tag{38}$$

The results show that the calculated results of the model are in good agreement with the experimental data, which proves that the new model can match the pre-peak behavior of sandstone samples under conventional triaxial loading. However, it should be noted that the damage variable is defined as the complete failure of the sandstone sample at peak stress, in fact the sample retains some strength after peak stress in the test.

5. Conclusions

In this study, triaxial compression tests were conducted on sandstone samples with pre-existing cracks at different angles. Based on the experimental data, the internal mechanisms of sandstone failure were explored theoretically, with a particular focus on the influence of crack angle on rock damage and failure. The main conclusions are as follows:

(1) The presence of cracks significantly impacts the mechanical properties of sandstone samples. The peak strength of cracked samples is notably lower than that of intact samples, with a decrease ranging from 53.85–64.67 %. As the crack angle increases, the peak strength rises monotonically, from 46.6 MPa at 0° to 60.9 MPa at 90°. This phenomenon can be explained by the variation of total absorbed energy and dissipated energy during sample damage.

(2) The crack volume strain can explain the damage fracture deformation law of fractured sandstone samples. The decrease and subsequent increase in crack volume strain indicate the closing, initiation, and expansion of internal cracks within the sample. When it is 0, the initial crack inside the sample is completely closed. According to this, the pre-peak process of progressive rock failure can be divided into crack closing compaction stage, linear elastic deformation stage and stable expansion stage. With the increase of crack Angle, crack initiation stress and damage stress decrease first and then increase. The sample with angle of 45° is the smallest, and the sample with angle of 90° is the largest.

(3) A mechanical model of crack propagation is established. Based on the maximum radial shear stress criterion, an analytical model of crack initiation angle and crack propagation is established. When tensile failure occurs, the crack propagates along the prefabricated crack direction. When shear failure occurs, the crack initiation angle is about 75°, and the deflection angle of the shear crack is about 123.8°. The theoretical analysis results explain the characteristics of sandstone failure modes under conventional triaxial compression.

(4) Based on the theory of damage mechanics and statistics, the damage related parameters m (damage rapid growth stage) and γ (damage variable growth rate) are introduced to construct the damage evolution expression, and the influence of crack angle on the sample damage speed is analyzed. With the increase of crack angle, m first increases and then decreases, and the sample with crack angle of 45° is the largest. γ decreases first and then increases, and the sample with crack angle of 45° is the smallest. The results shows that the slow damage growth stage is the longest, the damage increase rate is the fastest, and the damage failure is the fastest during loading.

(5) Combined with axial crack strain and damage variables, the damage constitutive model of sandstone samples under conventional triaxial loading is established. The theoretical results are basically consistent with the experimental data, which verifies the accuracy of the model.

CRediT authorship contribution statement

Hu Huarui: Writing – original draft, Funding acquisition, Data curation. **Zhang Xiang:** Resources, Formal analysis, Data curation. **Lu Jun:** Writing – review & editing, Methodology, Funding acquisition. **Zhu Chun:** Methodology, Data curation. **Liu Shiwei:** Resources, Data curation.

Declaration of Competing Interest

The authors declare that they have no known competing financial interests or personal relationships that could have appeared to influence the work reported in this paper.

Acknowledgements

This work was jointly supported by the Postdoctoral Fellowship Program of CPSF under Grant No. GZB20230451 and 2024T170578, National Natural Science Foundation of China Grant. No 52374222, National major science and technology project for deep earth Grant No.2024ZD1003903, Basic and Applied Basic Research Project of Guangdong Province (2024A1515010992).

References

[1] Y.Y. Lu, G.L. Zhao, Z.L. Ge, et al., Challenges and development direction of deep fragmented soft coalbed methane in China, Earth Energy Sci. (2024), https://doi.org/10.1016/j.ees.2024.08.001.
[2] W.J. Niu, K.G. Li, X.F. Liu, Failure mode and intelligent prediction method of thin-layered rock mass tunnel, Environ. Earth Sci. 84 (2025) 100.
[3] (a) X.T. Feng, C.X. Yang, R. Kong, et al., Excavation-induced deep hard rock fracturing: Methodology and applications, J. Rock. Mech. Geotech. 14 (1) (2022) 1–34;
(b) X.J. Yu, Y.P. Yang, X.F. Li, et al., Cracking formation and evolution in surrounding rock of a deep fractured rock mass roadway: a study of the 790-m level segment engineering at the Jinchuan Mine, China, Eng. Geol. 331 (2024) 107431.
[4] J.B. Li, M.C. Xie, S.L. Wang, et al., Study on the influence of thermo-pressure coupling environment on the fracture properties of shale in deep reservoirs, Theor. Appl. Fract. Mec. 131 (2024) 104440.
[5] P. Li, M.F. Cai, Challenges and new insights for exploitation of deep underground metal mineral resources, Trans. Nonferrous Met. Soc. China 31 (11) (2021) 3478–3505.
[6] G. Su, Y. Qin, H. Xu, et al., A sound-based machine learning method for crack-type recognition in hard rock, Bull. Eng. Geol. Environ. 82 (252) (2023), https://doi.org/10.1007/s10064-023-03291-4.
[7] Y.M. Zhao, X.T. Feng, Q. Jiang, et al., Large deformation control of deep roadways in fractured hard rock based on cracking-restraint method, Rock. Mech. Rock. Eng. 54 (2021) 2559–2580.
[8] C.W. Xin, F.X. Jiang, C.Z. Zhai, et al., Analysis of coal floor fault activation inducing water inrush using microseismic monitoring-a case study in Zhaogu No. 1 Coal Mine of Henan Province, China, Sustainability 15 (9) (2023) 7361.
[9] F.Q. Gong, P.L. Zhang, L. Xu, Damage constitutive model of brittle rock under uniaxial compression based on linear energy dissipation law, Int. J. Rock. Mech. Min. 160 (2022) 105273.
[10] F. Chen, J. Du, J. Lv, et al., Study on the size effect of rock burst tendency of red sandstone under uniaxial compression, Sci. Rep. 14 (2024) 16402.
[11] Q. Chen, Y. Liu, Z. Teng, et al., Investigations on the effect of natural veined calcite on the mechanical properties of limestone, Sci. Rep. 14 (2024) 5871.
[12] S. Luo, F.Q. Gong, L.L. Li, et al., Linear energy storage and dissipation laws and damage evolution characteristics of rock under triaxial cyclic compression with different confining pressures, T. Nonferr. Metal. Soc. 33 (7) (2023) 2168–2182.
[13] P.M. Li, L.S. Jiang, Z.J. Wen, et al., Effect of fractures on mechanical behavior of sand powder 3D printing rock analogue under triaxial compression, J. Cent. South Univ. 31 (2024) 2703–2716.

[14] I. Janeček, D.A. Mishra, C.S. Vishnu, et al., Experimental Study of Compact Sandstone Deformation Under Axisymmetric Triaxial Loading Along Specific Paths in Stress Space, Rock. Mech. Rock. Eng. 57 (2024) 97–113.
[15] Y. Zhang, Z.F. Wang, D.P. Xu, et al., True triaxial stresses mobilizing dilatant fracturing and engineering failure of hard rocks, Eng. Fail Anal. 154 (2023) 107652.
[16] F.Y. Wang, X.T. Feng, Y.Y. Zhou, et al., Experimental study on failure evolution mechanism of clastic rock considering cementation and intermediate principal stress, J. Rock. Mech. Geotech. 15 (7) (2023) 1636–1650.
[17] W.R. Abdellah, S.A. Bader, J.G. Kim, et al., Numerical simulation of mechanical behavior of rock samples under uniaxial and triaxial compression tests, Min. Miner. Depos. 17 (3) (2023) 1–11.
[18] H.D. Liu, J.J. Liu, S.Y. Zhang, et al., Experimental study on compression characteristics of fractured soft rock and its Mohr-Coulomb criterion, Theor. Appl. Fract. Mec. 125 (2023) 103820.
[19] K. Feng, X.P. Zhou, Peri dynamic simulation of the mechanical responses and fracturing behaviors of granite subjected to uniaxial compression based on CT heterogeneous data. Eng. Comput. 39 (2023) 307–329.
[20] P.H. Deng, Q.S. Liu, H.F. Lu, A novel joint element parameter calibration procedure for the combined finite-discrete element method, Eng. Fract. Mech. 276 (2022) 108924.
[21] H. Cao, D. Zhu, T. Bao, et al., Applicability of rock damage model based on power law distribution, Acta Geophys 72 (2024) 3021–3036.
[22] D. Huang, X.Q. Li, W.C. Song, Damage evolution and integrity assessment of jointed rock mass based on synthetic rock mass approach, KSCE J. Civ. Eng. 27 (2023) 2235–2247.
[23] K. Chen, M. Tang, Z. Guo, Comparative study on three-dimensional conventional and modified statistical damage constitutive models, Multiscale Multidiscip. Model. Exp. Des. 2 (2019) 259–267.
[24] S. Chajed, A. Singh, Acoustic Emission (AE) Based Damage Quantification and Its Relation with AE-Based Micromechanical Coupled Damage Plasticity Model for Intact Rocks, Rock. Mech. Rock. Eng. 57 (2024) 2581–2604.
[25] X.D. Xu, M.C. He, C. Zhu, et al., A new calculation model of blasting damage degree-Based on fractal and tie rod damage theory, Eng. Fract. Mech. 220 (2019) 106619.
[26] G. Chen, T. Li, G. Zhang, et al., Temperature effect of rock burst for hard rock in deep-buried tunnel, Nat. Hazards 72 (2014) 915–926.
[27] J. Chen, Y.B. Ye, Y.Y. Pu, et al., Experimental study on uniaxial compression failure modes and acoustic emission characteristics of fissured sandstone under water saturation, Theor. Appl. Fract. Mec. 119 (2022) 103359.
[28] W. Liu, K. Yang, L. Dou, et al., Mechanical properties and failure modes of CRCB specimen under impact loading, Sci. Rep. 12 (2022) 12108.
[29] C. Valle-Molina, L.A. Alcázar-Vara, J.J. Ordaz-Jiménez, et al., Rock characterization integrating free-free resonant column measurements and X-ray computed tomography imaging, Geomech. Geophys. Geo-Energ. Geo-Resour. 8 (2022) 164.
[30] H.B. Li, L.W. Liu, S.Y. Fu, et al., Rate-dependent strength and crack damage thresholds of rocks at intermediate strain rate, Int. J. Rock. Mech. Min. Sci. 171 (2023) 105590.
[31] X. Huang, C. Shi, H. Ruan, et al., Stable crack propagation model of rock based on crack strain, Energies 15 (5) (2022) 1885.
[32] R. Xu, S. Zhang, Z. Li, et al., Experimental investigation of the strain rate effect on crack initiation and crack damage thresholds of hard rock under quasi-static compression, Acta Geotech. 18 (2023) 903–920.
[33] X. Zhou, H. Yang, F. Berto, The micromechanics-based rate-dependent constitutive model of flawed rocks at intermediate strain rate, Fatigue Fract. Eng. M. 45 (6) (2022) 1807–1817.
[34] T. Qin, Y.W. Duan, H.R. Sun, et al., Mechanical characteristics and energy dissipation characteristics of sandstone under triaxial stress conditions, J. China Coal Soc. 45 (S1) (2020) 255–262.
[35] J.W. Hao, H.R. Li, W.G. Zhao, et al., Energy storage and fracture characteristics of brittle rock with rockburst proneness after microwave irradiation, Case Stud. Therm. Eng. 63 (2024) 105355.
[36] H.R. Hu, Y.Y. Lu, B.W. Xia, Damage characteristics of sandstone with different crack angles subjected to true triaxial cyclic loading and unloading, Theor. Appl. Fract. Mec. 121 (2022) 103444.
[37] J.P. Zuo, H.Q. Song, Y. Chen, et al., Post-peak progressive failure characteristics and nonlinear model of coal-rock combined body . , J. China Coal Soc. 43 (12) (2018) 3265–3272.
[38] J. Peng, G. Rong, M. Cai, et al., A model for characterizing crack closure effect of rocks, Eng. Geol. 189 (2015) 48–57.
[39] X.S. Liu, J.G. Ning, Y.L. Tan, et al., Damage constitutive model based on energy dissipation for intact rock subjected to cyclic loading, Int. J. Rock. Mech. Min. Sci. 85 (2016) 27–32.

Jun Lu is an assistant professor at the College of Civil and Transportation Engineering, Shenzhen University, Shenzhen, China. He won the title of Shenzhen Overseas High-level Talent. He obtained his PhD in Mining Engineering from Chongqing University in 2020. His main research interests cover the true triaxial rock mechanics, multifield coupling experimental technique, coal-rock dynamic disaster mechanism and prevention in deep engineering. He has presided over several national scientific research projects, published a few high-level academic papers, and has been awarded Chongqing outstanding doctoral thesis/Chinese Society of Rock Mechanics and Engineering exceptional doctoral thesis and other awards.